



1 **Impacts of Large-Scale Circulation on Urban Ambient Concentrations**
2 **of Gaseous Elemental Mercury in New York, USA**

3 Huiting Mao^{1†}, Dolly Hall², Zhuyun Ye¹, Ying Zhou¹, Dirk Felton³, and Leiming Zhang⁴

4 ¹Department of Chemistry, State University of New York College of Environmental Science and
5 Forestry, Syracuse, NY 13210

6 ²Department of Atmospheric and Oceanic Science, University of Maryland, College Park, MD
7 20742

8 ³Bureau of Air Quality Surveillance, Division of Air Resources, New York State Department of
9 Environmental Conservation, Albany, NY 12233

10 ⁴Air Quality Research Division, Science and Technology Branch, Environment and Climate
11 Change Canada, Toronto, M3H 5T4, Canada

12 [†]Correspondence to: hmao@esf.edu

13

14



15

Abstract

16 The impact of large-scale circulation on urban gaseous elemental mercury (GEM) was
17 investigated through analysis of 2008 – 2015 measurement data from an urban site in New York
18 City (NYC), New York, USA. Distinct annual cycles were observed in 2009-2010 with mixing
19 ratios in warm seasons (i.e. spring-summer) 10-20 ppqv (~10%-25%) higher than in cool seasons
20 (i.e. fall-winter). This annual cycle was disrupted in 2011 by an anomalously strong influence of
21 the North American trough in that warm season and was reproduced in 2014 with annual
22 amplitude enhanced up to ~70 ppqv associated with a particularly strong Bermuda High. North
23 American trough axis index (TAI) and intensity index (TII) were used to characterize the effect
24 of the North American trough on NYC GEM especially in winter and summer. The intensity and
25 position of the Bermuda High had a significant impact on GEM in warm seasons supported by a
26 strong correlation (r reaching 0.96, $p < 0.05$) of GEM with Bermuda High intensity indices in
27 summer. Regional influence on NYC GEM was supported by the GEM-carbon monoxide (CO)
28 correlation with r of 0.24-0.66 ($p \sim 0$) in most seasons and larger r in summers. Interannual
29 variations were found in simulated regional and local anthropogenic contributions, averaged at
30 ~75% (67%-83%) and 25% (17%-33%), respectively, to wintertime NYC anthropogenically
31 induced GEM concentrations. Results from this study suggest the possibility that the
32 increasingly strong Bermuda High over the past decades could dominate over anthropogenic
33 mercury emission control in affecting ambient concentrations of mercury via regional build-up
34 and possibly enhancing natural and legacy emissions.

35

36

37



38 1. Introduction

39 Atmospheric mercury (Hg) is a prevailing pollutant that has global consequences for both
40 human and ecosystem health, and hence Hg emission control is imperative. Mercury in the
41 atmosphere is operationally defined in three forms, gaseous elemental mercury (GEM), gaseous
42 oxidized mercury (GOM), and particulate-bound mercury (PBM). Total gaseous mercury (TGM)
43 is the sum of GEM and GOM. The most abundant of these three forms is GEM with a lifetime of
44 0.5 - 1 year (Driscoll et al., 2013) and mixing ratios on the order of hundreds of parts per
45 quadrillion (ppqv) (\sim a few ng m^{-3} at $1 \text{ ng m}^{-3} = 112 \text{ ppqv}$ in a standard atmosphere; unit
46 conversion was done in a standard atmosphere hereafter) compared to GOM and PBM with
47 lifetimes of hours to weeks and mixing ratios often on the order of single ppqv (\sim a few pg m^{-3}).

48 The median concentration of TGM/GEM in global continental remote areas was 1.6 ng
49 m^{-3} (180 ppqv) estimated from a large body of measurement studies (Mao et al., 2016), and the
50 background concentration of GEM in the Northern Hemisphere was $1.5 - 1.7 \text{ ng m}^{-3}$ (168 – 190
51 ppqv) (Lindberg et al., 2007). Urban concentrations of GEM/TGM in the U.S. varied over 0.05
52 – 324 ng m^{-3} (5.6 – 36288 ppqv) (Mao et al., 2016). In comparison, urban concentrations and
53 their temporal variability were larger than rural, remote, and high elevation concentrations in the
54 Northern Hemisphere (e.g., Kim and Kim, 2001; Feng et al., 2003; Denis et al., 2006; Liu et al.,
55 2007; Peterson et al., 2009; Sprovieri et al., 2010; Zhu et al., 2012; Lan et al., 2012, 2014; Chen
56 et al., 2013; Civerolo et al., 2014; Fu et al., 2015; Brown et al., 2015; Mao et al., 2016 and
57 references therein) owing to numerous controlling factors including anthropogenic and legacy
58 emissions, deposition, meteorology, transport, and atmospheric chemistry (Mao et al., 2016).

59 Over the United States measurements from the Atmospheric Mercury Network (AMNet)
60 sites, located in urban, suburban, rural, and remote areas, suggested that monthly median GEM



61 mixing ratios varied from 148 to 226 ppqv (~ 1.32 to 2.02 ng m⁻³) with urban values at the higher
62 end of the range (Lan et al., 2012). Urban ambient atmospheric TGM/GEM concentrations in
63 Canada on average ranged over $1.7 - 4.5$ ng m⁻³ ($190 - 504$ ng m⁻³) (Mao et al., 2016; reference
64 therein). Urban GEM/TGM concentrations in Asia could be an order of magnitude larger than
65 those in the U.S., Canada, and Europe (Mao et al., 2016; references therein). Many studies
66 identified local sources as a predominant factor controlling urban ambient concentrations
67 (Gabriel et al., 2005; Lyman and Gustin, 2009; Wang et al., 2013; Feng et al., 2003; Fang et al.,
68 2004; Zhu et al., 2012; Hall et al., 2014; Seo et al., 2016; Kim et al., 2016). In some urban
69 locations nighttime daily maximums and spring-summer annual peaks were attributed to local
70 and regional sources followed by boundary layer dynamics and meteorological conditions (Liu et
71 al., 2007; Cheng et al., 2009; Liu et al., 2010; Nair et al., 2012; Zhu et al., 2012). Surface
72 emissions were also suggested to play a major role in warm season annual maximums (Denis et
73 al., 2006; Zhu et al., 2012). Some sites experienced early morning daily maximums with the
74 strongest diurnal variation in summer, due possibly to local anthropogenic sources and surface
75 emissions (Stamenkovic et al., 2007; Peterson et al., 2009). Wintertime annual maximums were
76 attributed to less oxidation of GEM (Stamenkovic et al., 2007) and periods of cold and stagnant
77 air probably leading to build-up of pollution and more Hg evasion prompted by wet conditions
78 (Peterson et al., 2009). Temporal variations of GEM concentrations could be attributed to the
79 combined influence of environmental variables, anthropogenic sources, photochemistry, and
80 regional transport (Xu et al., 2014).

81 Some studies suggested that regional sources dominated over local ones in contributing to
82 urban ambient Hg concentrations (e.g., Liu et al., 2007; Kim et al., 2013; Engle et al., 2010; Xu
83 et al., 2014; Hall et al., 2014). On interannual time scales, the impact of regional transport, in



84 comparison to local sources, could vary greatly due to large variability in atmospheric circulation
85 and subsequently affect urban ambient concentrations very differently. Additional emission
86 control is anticipated in the future associated with the Mercury and Air Toxics Standards
87 (MATS) rule and the United Nations Environment Program (UNEP) international Minamata
88 Treaty (Selin, 2014). To regulate future emissions, it is important to understand and quantify
89 contributions of local versus regional sources to urban ambient concentrations. The objective of
90 this paper is to examine the seasonal, annual, and interannual variability of GEM in the Bronx
91 Borough of New York City (NYC) and its relation with large-scale circulation, and the
92 contributions of local and regional sources to NYC ambient GEM concentrations.

93 **2. Site Description, Measurement Data, and Analysis Methods**

94 The site discussed herein is maintained by the New York State Department of
95 Environmental Conservation (NYSDEC) as a part of AMNet under the National Atmospheric
96 Deposition Program (NADP). The site is located in a densely populated area of NYC, in the
97 borough of Bronx at the Pfizer Plant Research Laboratory within the New York Botanical
98 Garden (40.8679°N, 73.8781°W). The Bronx site is in close proximity to densely populated
99 local anthropogenic sources as well as downwind of many regional sources (Fig. 1).

100 GEM was measured every 5 minutes using a Tekran (Toronto, ON) model 2537B cold
101 vapor atomic fluorescence (CVAFA) analyzer with a nominal detection limit of $<0.1 \text{ ng m}^{-3}$ (~ 11.2
102 ppqv). The instrument was calibrated daily with an internal permeation source. The Tekran
103 system was operated according to standard operating procedures from the NADP's AMNet. The
104 AMNet site liaison performs annual site visits, which include manual injections to verify the
105 internal permeation source, and is responsible for quality assurance of the data (Civerolo et al.,
106 2014). Additional details can be found in Landis et al. (2002) and Gay et al. (2013).



107 Measurement data of sulfur dioxide (SO₂), nitrogen dioxide (NO₂), carbon monoxide
108 (CO), temperature, wind direction, and wind speed were averaged hourly. The SO₂
109 measurements were taken using a TEI 43C and a 43i TLE instrument using equivalent method
110 060 and pulsed fluorescence. The NO₂ measurements were taken using a TEI 42C instrument
111 using reference method 074 and chemiluminescence and catalytic conversion. CO was measured
112 by a TEI 48C and an API 300EU instrument using reference method 054 with non-dispersive
113 infrared absorption. The technical details of the deployment of these instruments are given by
114 the NYSDEC at www.dec.ny.gov/chemical/8541.html and in the 2016 Annual Monitoring
115 Network Plan (www.dec.ny.gov/docs/air_pdf/2016plan.pdf).

116 The impact of regional and local anthropogenic sources was simulated using the NOAA
117 Hybrid Single Particle Lagrangian Integrated Trajectory model (HYSPLIT) dispersion version
118 (Draxler and Hess, 1997, 1998; Draxler, 1999; Stein et al., 2015) for the winters and summers of
119 2009 – 2015. HYSPLIT was driven by the EDAS 40 km model output over a domain extending
120 westward to OH, southward to northern VA, and northward to include New England (Fig. 10a),
121 with a total of 522 counties reporting Hg emissions that were extracted from the Environmental
122 Protection Agency's National Emission Inventory 2011 ([https://www.epa.gov/air-emissions-](https://www.epa.gov/air-emissions-inventories/2011-national-emissions-inventory-nei-data)
123 [inventories/2011-national-emissions-inventory-nei-data](https://www.epa.gov/air-emissions-inventories/2011-national-emissions-inventory-nei-data)). Two emission scenarios of 120-hour
124 forward dispersion simulations were conducted for each day of a season. One included
125 emissions from all the 522 countries, and another excluded emissions from the five boroughs in
126 NYC. The difference in NYC GEM concentrations between the two scenarios was used to
127 approximate the effect of anthropogenic emissions in NYC (denoted as local sources) versus
128 outside of NYC (denoted as regional sources) on NYC ambient Hg concentrations, not
129 considering loss in transit.



130 In the analysis of the North American trough, the trough axis index (TAI) and trough
131 intensity index (TII) defined by Bradbury et al. (2002) were used to quantify the position and
132 intensity of the North American trough. The seasonal TAI quantifies the mean longitudinal
133 position of the quasi-stationary midtropospheric East Coast trough. The TAI domain extends
134 from 120°W to 30°W and the southern to northern boundaries ranged from 40°N to 50°N. The
135 TAI index was calculated by averaging the longitudinal positions (Lon) of the minimum 500-hPa
136 heights (H_{\min}) observed at each of the four latitudinal steps ($j=40^\circ, 42.5^\circ, 45^\circ, \text{ and } 47.5^\circ\text{N}$)
137 within the index range, to produce a practical index in longitudinal units (relative to the prime
138 meridian):

$$139 \quad \text{TAI} = \text{average} [\text{Lon}(H_{\min})_j]$$

140 The TII is an estimate of wave amplitude at 42.5°N and is the mean height change at the 500-hPa
141 surface from equal distances east and west of the East Coast trough axis. It was calculated:

$$142 \quad \text{TII} = \{[(H_{\min})_i - H_{i+30^\circ}] + [(H_{\min})_i - H_{i-30^\circ}]\}/2$$

143 The more negative TII is, the stronger the influence of the North American Trough would be.

144 The 2.5° x 2.5° reanalysis data from the National Center of Environmental Protection/National
145 Center of Atmospheric Research were used to calculate seasonal average TAI and TII.

146 Additional details about TAI and TII can be found in Bradbury et al. (2002).

147 **3. Results and Discussion**

148 **3.1 General Characteristics of Diurnal, Seasonal, and Interannual Variation**

149 Five-minute average GEM mixing ratios were more often larger during the warm seasons
150 (summer-spring) than the cool seasons (fall-winter) (Fig. 2), in agreement with previous urban
151 site studies (Denis et al., 2006; Liu et al., 2007; Zhu et al., 2012; Zhang et al., 2013; Civerolo et
152 al., 2014). The annual cycles were not as distinct and reproducible as those in rural



153 environments such as southern New England, where annual maximums were found in winter and
154 minimums in fall (Mao et al., 2008; Sigler et al., 2009; Mao and Talbot, 2012).

155 Three salient features were evident in the interannual variation of a range of percentile
156 mixing ratios of GEM (Fig. 3; Table 1). First, the 2009 – 2010 cool season percentile values of
157 GEM were the lowest of all cool seasons. Second, the 2011 warm season percentile values were
158 the lowest of all warm seasons, even lower than in the cool season of the same year, not
159 reproducing the 2009 and 2010 annual cycles. Third, the 2014 and 2015 seasonal percentile
160 values were mostly the highest of the study period and for the first time since 2011, warm season
161 values exceeded the cool season ones reproducing the 2009 and 2010 annual cycles.

162 The most pronounced diurnal cycles occurred in summer, as shown in seasonal average
163 diurnal cycles in Figure 4, with a peak between 02:00 and 06:00 UTC and a minimum between
164 10:00 and 16:00 UTC, which is consistent with previous studies for urban locations (e.g. Denis et
165 al., 2006; Liu et al., 2007; Zhu et al., 2012; Lan et al., 2012). In summers of 2009 – 2012, the
166 daily maximum was ~170-190 ppqv and the daily minimum ~140-160 ppqv. In summers of
167 2014 and 2015 mixing ratios were elevated greatly throughout the day with daily peaks reaching
168 ~200 and 290 ppqv and minimums ~180 and 225 ppqv, respectively. The diurnal amplitude,
169 defined as the difference between the daily maximum and minimum, was up to ~50 ppqv in
170 summer, ~20 ppqv in fall and spring, and <10 ppqv in winter.

171 During 2008 – 2013, the cool seasons experienced much larger interannual variability of
172 GEM than the warm seasons did, whereas in 2014 and 2015 GEM concentrations were elevated
173 significantly above other years in all seasons (Fig. 4). Over 2008 - 2013, the largest interannual
174 variability up to ~40 ppqv difference was observed between the lowest GEM mixing ratios in fall
175 2009 and largest in falls 2011 and 2012, whereas springs and summers experienced much less



176 interannual variability except spring and summer 2011, as aforementioned, that saw the lowest
177 GEM mixing ratios, ~ 20 ppqv lower than all other warm seasons.

178 **3.2. Interannual Variation of Cool Season GEM**

179 The 2009 – 2010 cool season exhibited the lowest percentile values whereas most of
180 winter 2014 and cool season 2014-2015 percentile values were the highest of the study period
181 (Table 1; Fig. 3). The difference in percentile values between the two cool seasons ranged from
182 33-34 ppqv in the 25th and median values to 112 ppqv in the 90th percentile value. The possible
183 effect of anthropogenic emission changes on those interannual variations in GEM concentrations
184 was the very first to be examined. EPA national emission inventories showed a 13% decrease
185 from 2008 (31810 kg) to 2011 (27695 kg), and then an increase of 2% to 2014 (28270 kg) in
186 total emissions from the Eastern US, including states east of the Mississippi River, of which
187 NYC emissions increased from 125 kg in 2008 to 145 kg in 2011 and to 199 kg in 2014
188 (<https://www.epa.gov/air-emissions-inventories/2014-national-emissions-inventory-nei-data>).
189 Using an average PBL height of 1000 m over the Eastern US (the surface area for the Eastern US
190 is $2.483 \times 10^{12} \text{ m}^2$), a decrease of 4115 kg from 2008 to 2011 emissions was converted to ~200
191 ppqv and averaged at ~0.2 ppqv d⁻¹ over all days of the three years, and an increase of 575 kg
192 from 2011 to 2014 emissions was converted to ~0.03 ppqv d⁻¹. The potential change in NYC
193 atmospheric concentrations were estimated to be ~3 ppqv d⁻¹ from the 2008 – 2011 NYC
194 emission increases alone and ~6 ppqv d⁻¹ from the 2011 – 2014 increase. The potential changes
195 in ambient concentrations caused by the regional emission decrease/increase were negligible
196 compared to the observed interannual difference. Those caused possibly by NYC emission
197 increases could be significant but appeared to be inconsistent with the changes in ambient
198 concentrations in two ways. First, from 2010 to 2011 NYC emissions increased and yet



199 summertime ambient concentrations decreased by 10 ppqv throughout the seasonal averaged
200 diurnal cycle (Fig. 4). Second, the observed increase from summer 2012 to summer 2014 was
201 nearly 90 ppqv throughout the seasonal averaged diurnal cycle, a factor of 15 larger than the
202 effect of the local emission rise as estimated above.

203 Legacy and natural emissions could be another driver for the observed interannual
204 variations in GEM. However, seasonal mean temperature and GEM from the Bronx location
205 were not found to be correlated, which suggested that the effect of changes in legacy and natural
206 emissions on ambient GEM might not be dominant. In addition, using Zhang et al. (2016)'s
207 estimated annual natural and reemissions 9.4 to $13.0 \mu\text{g m}^{-2}$ for the Bronx site during 2009-2014,
208 the maximum year-to-year change was calculated to be $\sim 1 \text{ ppqv d}^{-1}$ assuming an average
209 planetary boundary layer (PBL) height of 1000 m. This change alone could not explain the
210 observed interannual variations. It alludes to the potential effect of *regional* legacy and natural
211 emissions as well as chemistry, which needs to employ modeling tools and is beyond the scope
212 of this study. Here, it was hypothesized that atmospheric circulation was the predominant factor
213 causing interannual variation in Bronx ambient GEM concentrations.

214 To validate this hypothesis, circulation patterns were examined first using the Bronx site
215 wind data. In falls 2008, 2009, 2011, and 2013, wind came from all four quadrants with
216 comparable frequency ranging over 15% - 30% of the season, whereas in fall 2010 the
217 northwesterly (270° - 360°) was more frequent (37%), and the northeasterly (0° - 90°) became
218 predominant (~ 50 - 74%) in falls 2012 and 2014 (Fig. 5a). The winters experienced
219 northwesterly winds (270° - 360°) more often ranging from $\sim 40\%$ to 65% of the season with the
220 exception of winter 2015 when a little below 40% of the season on par with southwesterly wind
221 (180° - 270°) (Fig. 5a). Wind speed was averaged seasonally for the four wind quadrants (Fig.



222 5b). The strongest wind, reaching over 3 m s^{-1} , appeared in the northwesterly (270° - 360°) in
223 winter and spring from 2009 to 2013. Over 2014 and 2015 the most distinct change was
224 northwesterly wind speed being significantly reduced to a little over 2 m s^{-1} . The next in line was
225 southwesterly (180° - 270°) wind hovering around 2 m s^{-1} in the cool seasons except 2009-2010
226 when it was lowered to 1 m s^{-1} , nearly halved compared to other years. Wind speed in the two
227 easterly quadrants (0° - 180°) was comparable varying over $1 - 2 \text{ m s}^{-1}$ except that in spring 2013
228 it reached 2.5 m s^{-1} and was particularly low (0.5 m s^{-1}) in the 2014 cool season.

229 Since Hg sources are mostly concentrated to the west, southwest, south, and northeast of
230 the Bronx site with much fewer sources to the northwest (Fig. 1), GEM mixing ratios would vary
231 expectedly corresponding to air masses arriving from different directions. This was clearly
232 suggested by mixing ratios of GEM averaged seasonally for the four wind quadrants (Fig. 5c).
233 Generally, seasonally averaged GEM mixing ratios were larger by ~ 20 - 50 ppqv in the two
234 southerly than those in the northerly quadrants. One exception was summer 2014 when the
235 average concentration in the northeasterly quadrant reached up to 275 ppqv , and the frequency of
236 the northeasterly was the highest at 70% with average speed less than 1 m s^{-1} . Such weak wind
237 indicated fairly calm conditions in the region and the wind direction data were not meaningful.
238 Overall, in addition to local emissions, interannual variability in the origin of the air masses
239 reaching Bronx appeared to cast significant influence on the ambient concentrations of GEM in
240 the city.

241 Two cases, the lowest percentile values in the 2009–2010 cool season and the highest in
242 2014-2015, were used to elaborate on this point. What stood out in the 2009 – 2010 cool season
243 was very low frequency (14%) of wind from the southwesterly quadrant (180° - 270°) in fall 2009
244 and the largest frequency of wind from the northwesterly quadrant (67%, 270° - 360°) in winter



245 2010 combined with nearly the lowest wind speed ($\leq 1 \text{ m s}^{-1}$) in the three quadrants (0° - 270°)
246 (Figs. 5a-c). This indicated that the particularly low mixing ratios in the cool season of 2009 –
247 2010 were likely caused by over 4 times more frequent influx of relatively cleaner Canadian air
248 masses and slowest southerly flow of more polluted air.

249 The second case is winter 2014 when GEM averaged in the four wind quadrants reached
250 the maximums of all time respectively (Fig. 5c). Coincidentally the frequency of wind from the
251 northwesterly quadrant (270° - 360°) was nearly the lowest of all cool seasons barely reaching
252 40% of the season compared to up to 67% in winter 2010 (Fig. 5a). Meanwhile, the frequency of
253 wind from the southwesterly quadrant (180° - 270°) reached a high of 34% of all cool seasons,
254 and the wind speed of $\sim 2 \text{ m s}^{-1}$ was comparable to the northwesterly. This is a strong indication
255 of arrival of air masses rich in GEM originating from the heavy emitters in the Northeastern U.S.
256 Urban Corridor via flow nearly as frequent and as fast as the relatively clean northwesterly.
257 Winter 2015 showed similar wind patterns, also coincided with high GEM concentrations.

258 Such variations in wind direction and speed at the Bronx site can be better understood in
259 the context of large-scale circulation. The climatological 500 hPa geopotential height (GPH)
260 (1980-2010) for cool seasons during 1980-2010 exhibited the North American trough centered
261 over coastal southeastern Canada extending southwestward over the Eastern US (Fig. 6a). All
262 cool seasons experienced variations of this pattern except cool seasons 2009-2010 and 2013-
263 2014 that appeared to be anomalous (Figs. 6b and 6c). Specifically the trough in winter 2010
264 shifted eastward farthest out over the ocean and was the weakest, evidenced in the maximum
265 TAI (62°W) and nearly the least negative TII value (-80 m) (Fig. 6d). In contrast, the trough in
266 winter 2014 was situated the farthest over land and the strongest of all winters, backed by the
267 most negative TAI (85°W) and nearly the most negative TII value (-201 m) (Fig. 6d). This



268 suggested that in winter 2010 the Northeast US was most frequently under the influence of air
269 masses from higher latitudes via flow on the backside of the North American trough whereas
270 much less so due to the East U.S. positioned near the axis to the front of the trough in winter
271 2014. This was further clearly reflected in the maps of sea level pressure (SLP) for the two
272 winters. The unusual winter 2010 circulation was signified by northerly gradient flow (Fig. 6f)
273 from the backside of the Icelandic Low, which shifted toward the south and west near
274 Newfoundland compared to its 1980-2010 climatological position right between and below
275 Greenland and Iceland (Fig. 6e). This indicated predominant transport of relatively clean air
276 from Canada combined with strong ventilation of continental pollution, likely leading to the least
277 polluted air in winter 2010 of all 7 winters. In contrast, in winter 2014 NYC appeared to be on
278 the periphery of high pressure systems in predominantly slow northwesterly and southwesterly
279 flow regimes (Fig. 6g). This explains the least frequent, lowest wind speed in the easterly wind
280 quadrants during winter 2014 (Fig. 5b), which is conducive to regional build-up of air pollution,
281 resulting in the highest mixing ratios of GEM of all winters. More evidence was shown in
282 Section 6 using modeled contributions to NYC ambient concentrations from local versus
283 regional anthropogenic sources.

284 **3.3 Interannual Variation of Warm Season GEM**

285 **3.3.1 Annual maximums in warm seasons of 2009 and 2010**

286 The annual cycles of GEM at the Bronx site in 2009 and 2010, with larger values in
287 spring and summer (Table 1; Figs. 2 and 3), is consistent with measurements from some urban
288 and industrial locations in the literature (Lindberg and Stratton, 1998; Liu et al., 2007; Zhu et al.,
289 2012; Xu et al., 2014). Lindberg and Stratton (1998) and Liu et al. (2007) attributed such annual
290 cycles to local anthropogenic sources, while Zhu et al. (2012) and Xu et al. (2014) speculated



291 reemission from soils to be a potential dominant factor. In NYC, impervious surfaces comprise
292 95% of the total land surface (Adler and Tanner, 2013), which, considering local sources alone,
293 makes reemission of Hg from soils much less significant than anthropogenic emissions from the
294 area. Indeed no correlation between seasonal temperature and GEM was found for the Bronx
295 site as mentioned in Section 3.2. It thus seemed unlikely that NYC legacy emissions contributed
296 to the 2009 and 2010 annual cycles. The impact of regional vs. local anthropogenic sources on
297 NYC GEM concentrations was studied in Section 6, and quantifying the impact of *regional*
298 natural and legacy emissions calls for a regional modeling approach, which is beyond the scope
299 of this study. Here we focused on the potential impact of circulation on NYC GEM
300 concentrations.

301 In the warm seasons, Bronx was on the periphery of the Bermuda High in transition to
302 under the influence of the North American trough, and consequently Bronx was, as most of the
303 eastern US was, more frequently under the high pressure system influence (Figs. 7c,f), which is
304 usually lower wind speed. This is consistent with the annual cycle of wind speed shown in
305 Figure 5b, with wind mostly lower in spring-summer and higher in fall-winter conducive to
306 regional pollution build-up, which could explain why Bronx saw larger peaks of GEM in the
307 warm season than in the cool season.

308 **3.3.2 Lowest GEM in warm season 2011 and highest in 2014**

309 In examining wind in the warm season 2011, what stood out was that Bronx experienced
310 significantly increased frequency (37%) of northeasterly wind at wind speed nearly 2 m s^{-1} in
311 spring and decreased frequency of (20%) of northwesterly wind in summer compared to the
312 spring and summer in 2009 and 2010 (Fig. 5a). In summer 2014 nearly 80% of the season had
313 northeasterly wind (0° - 90°) and there was unusually weak wind ($\sim 1 \text{ m s}^{-1}$) in all four wind



314 quadrants (Figs. 5a,b), which suggested calm conditions. In summer 2011 GEM concentrations
315 in the northeasterly wind quadrant were averaged ~ 145 ppqv, ~ 30 ppqv lower than that in the
316 most polluted southerly quadrants (Fig. 5c). In contrast, summer 2014 GEM in the northeasterly
317 quadrant was averaged 275 ppqv compared to $\sim 160 - 200$ ppqv in the other three quadrants (Fig.
318 5c). The unusually high concentration was an indication of build-up under calm conditions.

319 The anomalously increased occurrence of northeasterly wind in summer 2011 indicated
320 unusual circulation. Compared to the 1980-2010 climatology, the 500 hPa GPH in spring 2011
321 showed the weakest North American trough of all springs (Fig. S1), evidenced in the
322 westernmost trough axis position (TAI = 108°W) and the smallest intensity (TII = -27 m) of all
323 springs (Fig. 7a). The 500 hPa GPH in summer 2011 suggested the strongest North American
324 trough (TII = -87 m) and the second easternmost trough axis position (TAI = 66°W) of all
325 summers (Fig. 7b; Fig. S2). This suggested that the Northeast U.S. in summer 2011 was
326 frequently under significant influence of the backside of the trough, i.e. sweeping air flow from
327 higher latitudes subsiding to the surface in midlatitudes.

328 Near the surface, the 1980-2010 SLP climatology suggested that in spring NYC was
329 situated in the gradient flow of the Bermuda High and a trough from the Icelandic Low (Fig. 7c),
330 conducive to transport of emissions from upstream source regions such as upstate New York,
331 Ohio (OH) and Pennsylvania (PA), while in summer under the influence of the Bermuda High
332 favorable to regional build-up (Fig. 7f). However, in spring 2011, the trough of the Icelandic
333 Low gave way to the Canadian High leaving NYC locked in a zone between the Canadian High
334 and subtropical high (Fig. 7d), possibly cutting regional transport short in addition to strong
335 subsidence of cleaner higher latitudinal air leading to the lowest concentrations of GEM of all
336 springs. Similarly unusual was summer 2011 when NYC was under less influence of the



337 Bermuda High than that of the North American Trough unfavorable to regional build-up (Figs.
338 7g). These speculations appeared to be consistent with the fact that both seasons saw unusual
339 equal chances of winds from the four quadrants (Fig. 5a) over Bronx and its surrounding areas.

340 The 500 hPa TAI and TII values (Figs. 7b) and the 500 hPa GPH map in summer 2014
341 (Fig. S2) suggested the weakest North American trough (TII = -44 m) of all summers, with its
342 axis on average at 72°W, near the East Coast. This indicates that summer 2014 experienced the
343 strongest influence of the Bermuda High on the East Coast (Figs. 7e,h) of all summers during the
344 study period, the polar extreme of the 2011 warm season. Corresponding to that, the summer
345 2014 SLP map (Fig. S4) exhibited the Bermuda High ridge over the Eastern U.S. more north-
346 extending than in other years, which is consistent with weak winds in all directions as shown in
347 Fig. 5b. This dynamic situation led to regional build-up conducive to the highest GEM mixing
348 ratios in all wind quadrants.

349 To be quantitative, domain (25°N-50°N, 95°W-70°W) average SLP was used as an
350 indicator to gauge the influence of the Bermuda High, and the number of grids with SLP
351 exceeding 1014 hPa over the domain, the northernmost latitude, and westernmost longitude of
352 the 1014 hPa isobar were used to gauge the horizontal spatial extent of the influence of the
353 Bermuda High. These four indices for the summers of 2009 – 2015 were plotted together with
354 summertime median mixing ratios of GEM in Figure 8. The summertime median mixing ratio of
355 GEM was correlated with the four indices at r ranging over 0.84 – 0.96 ($p = 0.06 - 0.009$), best
356 correlated with the northernmost latitude that the 1014 hPa isobar reached at $r=0.96$ ($p=0.009$).
357 The lowest GEM in summer 2011 was associated with the weakest influence of the Bermuda
358 High indicated by its smallest spatial extent, reflected in the lowest domain averaged SLP (1013
359 hPa), the fewest grids with SLP > 1014 hPa (44), and the southernmost latitude (37°N) the 1014



360 hPa isobar reached. The trough over the East Coast reached its southernmost point down to
361 North Carolina compared to other summers (Fig. S4), indicating more widespread influence of
362 relatively clean Canadian air on the Eastern US sweeping out the heavily polluted air in the
363 region. One may argue that the positive correlations shown above appeared to be driven by one
364 point in summer 2014, due to missing/unavailable data in summers 2013 and 2015. It should be
365 noted that the dramatic increase in GEM in summer 2014 needs to be put in the perspective of
366 the seasons proceeding and following summer 2014, when GEM was increased consistently in
367 seasons from winter 2014 through spring 2015 compared to all previous years. Therefore, the
368 large increase in summer 2014 was most likely not fortuitous, and more importantly such
369 increases were consistent with the driving physical mechanisms as suggested in the large scale-
370 circulation.

371 It should be noted that the seasonal median GEM values in the four wind quadrants
372 exhibited trends largely consistent with those in the overall seasonal values ($r=0.71 - 0.93, p \sim 0$),
373 and the ones in the more polluted southerly quadrants were slightly more so ($r=0.93, p \sim 0$) (Fig.
374 5c). This suggests that changes in ambient mixing ratios occurred in air masses coming from all
375 directions, whether they were from the relatively clean northwest and northeast, or the heavily
376 polluted regions southeast and southwest of Bronx. This was perhaps because the lifetime of
377 GEM is long enough for air from all wind directions to be regionally mixed. Overall, the fact
378 that the GEM values in the two relatively more polluted quadrants were correlated with the
379 overall values suggested that the trend in the ambient GEM mixing ratio was possibly associated
380 in large part with changes in anthropogenic emissions.

381 **4. Relationships Between GEM and Anthropogenic Tracers**

382 Correlations between Hg and several tracers (e.g., CO, SO₂, and NO₂) have been



383 commonly used to identify Hg anthropogenic sources, source-receptor relationships, and/or
384 emission ratios. The linear correlation between CO and GEM, especially in winter, in rural
385 locations despite their different sources, reflects their emission ratios in regionally well-mixed air
386 masses (e.g., Mao et al., 2008). At the Bronx site, seasonal GEM and CO were found to be
387 correlated with r up to 0.66 ($p \sim 0$) in all seasons over 2008 –2013, indicating significant, year-
388 round *regional* influence, and the two were notably not correlated in all the seasons from winter
389 2014 through spring 2015. Over 2008 – 2013 r^2 values of GEM-CO were larger in warm than in
390 cold seasons with the maximums exceeding 0.40 in spring 2010 and winter – summer 2011 (Fig.
391 9). The slope value varied from the smallest (~ 0.14 ppqv ppbv⁻¹) in spring-summer 2010 to the
392 largest (0.21 ppqv ppbv⁻¹) in summer 2012 (Fig. 9), close to and higher than the upper end of the
393 range, 0.06 – 0.14 ppqv ppbv⁻¹, from rural southern New Hampshire (NH) during winters 2004 –
394 2007 (Mao et al., 2008). This was greatly different from the GEM-CO correlation in rural
395 southern NH in winter only due to confounding factors such as legacy emissions and wet
396 deposition in summer (Mao et al., 2008; Lombard et al., 2011). Bronx experiencing more
397 significant GEM-CO correlation in warm seasons indicated better regionally mixed air masses,
398 influenced predominantly by anthropogenic emissions, than in cool seasons. This is consistent
399 with the cool and warm seasonal circulation patterns as discussed in Sections 3.2 and 3.3, which
400 is that in warm seasons NYC was predominantly under the influence of the subtropical high
401 conducive to regional mixing and build-up of pollutants.

402 No correlation between GEM and CO over 2014 – 2015 could be due in part to the more
403 dramatic emission reductions in CO than changes in GEM in the Eastern U.S. The high
404 percentile values of CO at the Bronx site had been affected by anthropogenic emission
405 reductions over the years, while the 10th and 25th percentile values remained fairly constant in all



406 seasons (Fig. S5). Zhou et al. (2015) suggested that baseline CO in Northeastern US rural areas
407 was controlled by a multitude of factors including global biomass emissions, large-scale
408 circulation, and cyclone activity. At the Bronx site, the low percentile value, close to regional
409 baseline levels, was possibly determined by a range of factors, whose importance could have
410 varied from year to year.

411 Unlike previous studies (e.g., Jen et al., 2013; Choi et al., 2013), GEM at the Bronx site
412 was found hardly correlated with SO₂ while somewhat to moderately correlated with NO₂ ($r =$
413 $0.22 - 0.64$, $p < 0.0001$) (Table 2), despite abundant sources co-emitting GEM, SO₂, and NO₂
414 locally and upwind. In addition to different lifetimes, different magnitude and timing of
415 emission reduction implementations and source types of the three compounds could have
416 affected their relation. Total Hg anthropogenic emissions in NYC were increased by 16% from
417 2008 to 2011, mainly in miscellaneous non-industrial NEC and waste disposal emissions, and
418 further increased by 37% from 2011 to 2014 primarily in fuel combustion. As aforementioned,
419 emissions of Hg in the Eastern U.S. decreased by 13% from 2008 to 2011 and increased by 2%
420 from 2011 to 2014. In contrast, total SO₂ emissions in NYC decreased steadily by 30% from
421 2008 to 2011 followed by a further decrease of 43% to 2014, while over the Eastern U.S
422 decreased by 48% from 2008 to 2011 and furthered by another 29% decrease in 2014. The effect
423 of these decreases in SO₂ emissions was reflected in the Bronx data, with a 58% decrease in the
424 seasonal median mixing ratio of SO₂ from 9.2 ppbv in winter 2009 to 2.8 ppbv in winter 2015
425 (Fig. S6). As for NO₂, fuel and mobile combustion emissions comprised >99.5% of the total
426 NO_x emissions in NYC and ~90% over the Eastern US. NYC NO_x emissions changed
427 insignificantly (1%) from 2008 to 2011 and by 15% from 2011 to 2014, while Eastern US
428 mobile and fuel combustion emissions were decreased by 16% and 33%, respectively, from 2008



429 to 2011, and further decreased by 13% and 9%, respectively, to 2014. These varying changes
430 possibly contributed to confounding the emission signature of GEM vs. NO_x and altered that of
431 GEM vs SO_2 .

432 The effect of local emissions can be accentuated by the correlation between GEM and
433 SO_2 and between GEM and NO_2 for the SO_2 and NO_2 mixing ratios exceeding their respective
434 seasonal 95th percentile concentrations. However, nearly no correlation between GEM and SO_2
435 as well as between GEM and NO_2 was found in this subset of data (Table 2). It should therefore
436 be cautioned that tracer correlation could not be used to identify source types of GEM or
437 estimate emission ratios of GEM to SO_2 or NO_2 in NYC.

438 **5. Regional vs. Local Contributions to NYC Ambient GEM Concentrations**

439 HYSPLIT dispersion simulations were used to obtain a quantitative comparison of the
440 effects of sources outside and inside NYC on NYC ambient concentrations of GEM. As stated
441 in Section 2, the modeling domain extended westward to OH and southward to northern VA, and
442 northward to include New England (Fig. 10a), with a total of 522 counties reporting Hg
443 emissions. Shown in Figure 10b is the contribution, in percentage of the total contribution from
444 all anthropogenic emissions in the domain, to NYC ambient concentrations of GEM from
445 anthropogenic emissions alone from local sources, and in Figure 10c is the contribution of
446 emissions from regional anthropogenic sources. There was clearly interannual variability in the
447 contribution of local versus regional anthropogenic sources. Local emissions averaged a
448 contribution of 25% in all winters of 2009 – 2015 with the period minimum of 17% in winter
449 2011 and the maximum of 33% in winter 2013 (Fig. 10b). Conversely, the contribution of
450 regional sources averaged a contribution of 75% in all winters with the largest 83% in winter
451 2011 and the lowest 67% in winter 2013 (Fig. 10c). Compared to that in the winter of the same



452 year, contributions from local sources were larger (by up to 12% in 2009) in summer 2009, 2011,
453 2012, and 2014, close in summer 2010, and 10% smaller in summer 2013 (Fig. 10b).

454 A close examination revealed largely consistent relation between NYC GEM mixing
455 ratios and source contributions. As suggested in Section 3.2, Bronx in winter 2010 experienced
456 the lowest concentrations of GEM in all percentile values, and yet, interestingly the simulated
457 local contribution in winter 2010 was in the mid-range of the 7 winters. This indicates that the
458 particularly low background concentration in the sweeping northerly flow led to less regional
459 contribution to NYC Hg concentrations than regional sources would in other years. In contrast,
460 winter 2014 saw the highest 25th, 50th, 75th, and 90th percentile concentrations of GEM, and yet
461 the contribution of local sources (~22%) was not even higher than average (25%). As
462 aforementioned, in winter 2014 the Eastern U.S. was most likely under the least dynamic
463 conditions conducive to regional build-up of air pollution, which resulted in a higher than
464 average contribution from regional sources and conversely lower than average contribution from
465 local sources (Fig. 10c). Consistent with GEM, the lower percentile mixing ratios of CO, SO₂,
466 and NO₂ appeared to be elevated or stopped decreasing compared to those in the previous year
467 (Figs. S5,S6).

468 The HYSPLIT dispersion model simulations suggested that close to three quarters of the
469 anthropogenically induced concentration of GEM in NYC was from regional sources. It should
470 be noted that to save computational time, the simulation domain used in this study was smaller
471 than ideal. With a larger regional domain, the significance of regional anthropogenic sources
472 could be enhanced. In addition, other factors/processes might have competed with the effect of
473 anthropogenic emission reductions, such as legacy and natural emissions, deposition,
474 meteorology, and/or large-scale circulation. Nearly 90% of the model simulation domain is



475 covered by vegetation. SMOKE model output in Ye et al. (2017) suggested that the ratio of
476 anthropogenic to legacy and natural emissions was 0.3 over the domain. Legacy and natural
477 emissions could become dominant under warmer and wetter conditions in summer. Moreover,
478 Hg deposition could be impacted by changes in physical parameters such as light, temperature,
479 and plant species (Rutter et al., 2011). Indeed changes of -30% to 50% in Hg deposition were
480 simulated for the Eastern US from the 2000s to the 2050s due to changes in precipitation
481 (Megaritis et al., 2014). Net GEM surface emissions were estimated to be dominant in summer
482 and net dry deposition in other seasons at majority of AMNet monitoring sites in eastern North
483 America (Zhang et al., 2016). Since Hg deposition and legacy emissions are closely linked,
484 these studies indicate potential changes in legacy emissions in response to variable
485 meteorological conditions and changing climate with subsequent effects on atmospheric Hg
486 concentrations. Therefore, with legacy and natural emissions accounted for, regional
487 contributions to NYC ambient Hg concentrations would be even more dominant.

488 **6. Summary**

489 For the Bronx site in NYC, distinct annual cycles of GEM were found in 2009 and 2010
490 with higher concentrations in warm than in cool seasons by 10 – 20 ppqv (~10% – 25%),
491 consistent with urban annual cycles reported in the literature. This annual cycle was not
492 reproduced in 2011 with anomalously low concentrations in the warm season and occurred again
493 in 2014 with significantly enhanced annual amplitude up to ~70 ppqv. Such temporal variability
494 in the urban GEM concentration was found to be driven by that in large-scale circulation.
495 Seasonal median mixing ratios of GEM was found to be correlated with both the North
496 American TAI and TII in winter and with TII in summer. Further, the intensity and position of
497 the Bermuda High pressure system had a significant impact on Bronx GEM concentrations in



498 warm seasons. This was evidenced in the strong correlation ($r = 0.84 - 0.96$, $p = 0.06 - 0.009$) of
499 seasonal median mixing ratios of GEM with four Bermuda High intensity indices, best correlated
500 at $r = 0.96$ ($p = 0.009$) with the northernmost latitude that the 1014 hPa isobar reached. The year of
501 2014 experienced anomalously strong influence of the Bermuda High resulting in the largest
502 GEM mixing ratios of the entire study period in all percentile values throughout the year. The
503 regional influence on GEM concentrations in Bronx was corroborated by significant, year-round
504 GEM-CO correlation (r up to 0.66, $p \sim 0$) over 2008 - 2013. This correlation disappeared
505 completely from winter 2014 through spring 2015 possibly resulting from their very different
506 emission changes in the Eastern U.S.

507 HYSPLIT dispersion model simulations suggested that regional sources outside of NYC
508 contributed to $\sim 75\%$ (67% - 83%) of the anthropogenic portion of the ambient GEM
509 concentration and NYC emissions the remaining $\sim 25\%$ (17% - 33%). Significant interannual
510 variation in the regional and local contributions was found to be consistent with that in large-
511 scale circulation. The fact that there was no clearly defined trend in GEM concentrations at the
512 Bronx site during the study period, despite decreases anthropogenic emission reductions in the
513 Eastern U.S. from 2008 to 2014, suggested that other factors/processes, such as large-scale
514 circulation and legacy/natural emissions, might have dominated over anthropogenic emission
515 reductions.

516 The North Atlantic Subtropical High over 1978 - 2007 had reportedly become more
517 intense, and its western ridge had displaced westward with an enhanced meridional movement
518 (Li et al., 2011). The increasing intensity and spatial extent of the high pressure system could
519 cast a strong influence on the Northeastern US with subsequent effect on ambient concentrations
520 of Hg via regional build-up and changing legacy emissions. This could dominate over the effect



521 of anthropogenic emission reductions, as suggested by this study. Indeed Zhu and Liang (2013)
522 recommended that strong decadal variations in the Bermuda High should be considered in the
523 U.S. air quality dynamic management. Therefore controlling urban ambient concentrations of
524 Hg needs to account for the overall impact of multiple factors, which may not be dominated by
525 emission reductions.

526 **Acknowledgments**

527 This work was funded by the Environmental Protection Agency Grant Agreement
528 #83521501. We are grateful to M. L. Olson and T. R. Bergerhouse of NADP & University of
529 Illinois at Urbana-Champaign and K. Civerolo of NYS DEC for making the Bronx GEM data
530 available. We also thank K. Civerolo for helpful comments. The authors gratefully
531 acknowledge the NOAA Air Resources Laboratory for free access to HYSPLIT. The
532 measurement data used in this study could be obtained from AMNet of NADP
533 (<http://nadp.sws.uiuc.edu/amn/data.aspx>).

534 **References**

- 535 Adler, F. R., and Tanner, C. J.: Urban Ecosystems: Ecological Principles for the Built
536 Environment, 353 pages, Cambridge University Press; 1st edition, 2013.
- 537 Bradbury, J. A., Keim, B. D., and Wake, C. P.: U.S. East Coast Trough Indices at 500 hPa and
538 New England Winter Climate Variability, *J. Clim.*, 15, 3509-3517, 2002.
- 539 Brown, R. J. C., Goddard, S. L., Butterfield, D. M., Brown, A. S., Robins, C., Mustoe, C. L., and
540 McGhee, E. A.: Ten years of mercury measurement at urban and industrial air
541 quality monitoring stations in the UK, *Atmos. Environ.*, 109, 1-8, 2015.
- 542 Chen, L., M. Liu, Z. Xu, R. Fan, J. Tao, D. Chen, D. Zhang, D. Xie, and J. Sun: Variation trends
543 and influencing factors of total gaseous mercury in the Pearl River Delta - A highly



- 544 industrialized region in South China influenced by seasonal monsoons, *Atmos. Environ.*, 77,
545 757-766, 2013.
- 546 Cheng, I., Lu, J., and Song, X.: Studies of potential sources that contributed to atmospheric
547 mercury in Toronto, Canada, *Atmos. Environ.*, 43, 6145–6158, 2009.
- 548 Choi, H., Huang, J., Mondal, S., and Holsen, T. M.: Variation in concentrations of three mercury
549 (Hg) forms at a rural and a suburban site in New York State, *Sci. Total Environ.*, 448, 96-
550 106. doi:10.1016/j.scitotend.2012.08.052, 2013.
- 551 Civerolo, K. L., Rattigan, O. V., Felton, D. H., Hirsch, M. J., and DeSantis, S.: Mercury wet
552 deposition and speciated air concentrations from two urban sites in New York State;
553 temporal patterns and regional context, *Aeros. Air Qual. Res.*,
554 doi:10.4209/aaqr.2014.03.0052, 2014.
- 555 Denis, M. S., Song, X., Lu, J. Y., and Feng, X.: Atmospheric gaseous elemental mercury in
556 downtown Toronto, *Atmos. Environ.*, 40(21), 4016-4024,
557 doi:10.1016/j.atmosenv.2005.07.078, 2006.
- 558 Draxler, R. R. (1999), HYSPLIT4 user's guide, NOAA Tech. Memo. ERL ARL-230, NOAA Air
559 Resources Laboratory, Silver Spring, MD.
- 560 Draxler, R. R., and Hess, G. D.: An overview of the HYSPLIT_4 modeling system of
561 trajectories, dispersion, and deposition, *Aust. Meteor. Mag.*, 47, 295-308, 1998.
- 562 Draxler, R. R., and Hess, G. D.: Description of the HYSPLIT_4 modeling system, NOAA Tech.
563 Memo. ERL ARL-224, NOAA Air Resources Laboratory, Silver Spring, MD, 24 pp, 1997.
- 564 Driscoll, C. T., Mason, R. P., Chan, H. M., Jacob, D. J., and Pirrone, N.: Mercury as a global
565 pollutant: sources, pathways, and effect, *Environ. Sci. Technol.*, 47, 4967–4983, 2013.



- 566 Engle, M. A., Tate, M. T., Krabbenhoft, D. P., Schauer, J. J., Kolker, A., Shanley, J. B., and
567 Bothner, M. H.: Comparison of atmospheric mercury speciation and deposition at nine sites
568 across central and eastern North America, *J. Geophys. Res.-Atmos.*, 115,
569 doi:10.1029/2010JD014064, 2010.
- 570 Fang, F., Wang, Q., and Li, J.: Urban environmental mercury in Changchun, a metropolitan city
571 in Northeastern China: source, cycle, and fate, *Sci. Total Environ.*, 330, 159 – 170, 2004.
- 572 Feng, X., Tang, S., Shang, L., Yan, H., Sommar, J., and Lindqvist, O.: Total gaseous mercury in
573 the atmosphere of Guiyang, P. R. China, *Sci. Total Environ.*, 304, 61 – 72, 2003.
- 574 Fu, X. W., Zhang, H., Yu, B., Wang, X., Lin, C.-J., and Feng, X. B.: Observations of atmospheric
575 mercury in China: a critical review, *Atmos. Chem. Phys.*, 15, 9455–9476, doi:10.5194/acp-
576 15-9455-2015, 2015.
- 577 Gabriel, M. C., Williamson, D. G., Brooks, S., and Lindberg, S.: Atmospheric speciation of
578 mercury in two contrasting Southeastern US airsheds, *Atmos. Environ.*, 39, 4947–4958,
579 2005.
- 580 Gay, D. A., Schmeltz, D., Prestbo, E., Olson, M., Sharac, T. and Tordon, R.: The Atmospheric
581 Mercury Network: Measurement and Initial Examination of an Ongoing Atmospheric
582 Mercury Record across North America, *Atmos. Chem. Phys.*, 13, 11339–11349, 2013.
- 583 Hall, C. B., Mao, H., Ye, Z., Talbot, R., Ding, A., Zhang, Y., Zhu, J., Wang, T., Lin, C. J., Fu,
584 C., and Yang, X.: Sources and dynamic processes controlling background and peak
585 concentrations of TGM in Nanjing, China, *Atmosphere*, 5(1), 124-155, 2014.
- 586 Jen, Y.-H., Yuan, C.-S., Hung, C.-H., Ie, I.-R., and Tsai, C.-M.: Temporal Variation and
587 Partition of Atmospheric Mercury during Wet and Dry Seasons at Sensitivity Sites within a
588 Heavily Polluted Industrial City, *Aeros. Air Quality Res.*, 13, 13-23, 2013



- 589 Kim, K. H., and Kim, M. Y.: The temporal distribution characteristics of total gaseous mercury
590 at an urban monitoring site in Seoul during 1999–2000, *Atmos. Environ.*, 35, 4253–4263,
591 2001.
- 592 Kim, K. H., Yoon, H. O., Brown, R. J., Jeon, E. C., Sohn, J. R., Jung, K., Park, C. G., and Kim,
593 I. S.: Simultaneous monitoring of total gaseous mercury at four urban monitoring stations in
594 Seoul, Korea, *Atmos. Res.*, 132, 199-208, 2013.
- 595 Kim, K.-H., Brown, R. J., Kwon, E., Kim, I.-S., and Sohn, J.-R.: Atmospheric mercury at an
596 urban station in Korea across three decades, *Atmos. Environ.*, 131, 124-132, 2016.
- 597 Landis, M. S., Stevens, R. K., Schaedlich, F. and Prestbo, E. M.: Development and
598 Characterization of an Annular Denuder Methodology for the Measurement of Divalent
599 Inorganic Reactive Gaseous Mercury in Ambient Air. *Environ. Sci. Technol.*, 36, 3000–
600 3009, 2002.
- 601 Lan, X., Talbot, R., Castro, M., Perry, K., and Luke, W.: Seasonal and diurnal variations of
602 atmospheric mercury across the US determined from AMNet monitoring data, *Atmos. Chem.*
603 *Phy.*, 12(4), 10569-10582. doi:10.5194/acp-12-10569-2012, 2012.
- 604 Lan, X., Talbot, R., Laine, P., Lefer, B., Flynn, J., and Torres, A.: Seasonal and diurnal
605 variations of total gaseous mercury in urban Houston, TX, USA, *Atmosphere*, 5, 399–419,
606 2014.
- 607 Li, W., Li, L., Fu, R., Deng, Y., and Wang, H.: Changes to the North Atlantic Subtropical High
608 and Its Role in the Intensification of Summer Rainfall Variability in the Southeastern United
609 States, *J. Clim.*, 24(5), 1499-1506, 2011.
- 610 Lindberg, S., Bullock, R., Ebinghaus, R., Engstrom, D., Feng, X., Fitzgerald, W., Pirrone, N.,
611 Prestbo, E., and Seigneur, C.: A synthesis of progress and uncertainties in attributing the



- 612 sources of mercury in deposition, *Ambio*, 36(1), 19-32, 2007.
- 613 Lindberg, S. E., and Stratton, W. J.: Atmospheric mercury speciation: concentrations and
614 behavior of reactive gaseous mercury in ambient air, *Environ. Sci. Technol.*, 32, 49–57,
615 1998.
- 616 Liu, B., Keeler, G. J., Dvonch, J. T., Barres, J. A., Lynam, M. M., Marsik, F. J., and Morgan, J.
617 T.: Temporal variability of mercury speciation in urban air, *Atmos. Environ.*, 41(9), 1911-
618 1923. doi:10.1016/j.atmosenv.2006.10.063, 2007.
- 619 Liu, B., Keeler, G. J., Dvonch, J. T., Barres, J. A., Lynam, M. M., Marsik, F. J., and Morgan, J.
620 T.: Urban-rural differences in atmospheric mercury speciation, *Atmos., Environ.*, 44, 2013-
621 2023, 2010.
- 622 Lyman, S. N., and Gustin, M. S.: Determinants of atmospheric mercury concentrations in Reno,
623 Nevada, USA, *Sci. Total Environ.*, 408(2), 431-438, 2009.
- 624 Lombard, M. A. S., Bryce, J., Mao, H., and Talbot, R.: Mercury deposition in southern New
625 Hampshire, 2006 - 2009, *Atmos. Chem. Phys.*, 11, 7657–7668, www.atmos-chem-
626 phys.net/11/7657/2011/doi:10.5194/acp-11-7657-2011, 2011.
- 627 Mao, H., Talbot, R., Sigler, J. M., Sive, B. C., and Hegarty, J. D.: Seasonal and diurnal variation
628 in Hg⁰ over New England, *Atmos. Chem. Phys.*, 8, 1403-1421, 2008.
- 629 Mao, H., and Talbot, R.: Long-term variation in speciated mercury at marine, coastal and inland
630 sites in New England: Part I Temporal Variability, *Atmos. Chem. Phys.*, 12, 5099-5112,
631 doi:10.5194/acp-12-5099-2012, 2012.
- 632 Mao, H., Cheng, I., and Zhang, L.: Current understanding of the driving mechanisms for
633 spatiotemporal variations of atmospheric speciated mercury: a review, *Atmos. Chem. Phys.*,
634 16, 1–28, 2016, www.atmos-chem-phys.net/16/1/2016/, doi:10.5194/acp-16-1-2016, 2016.



- 635 Megaritis, A. G., Murphy, B. N., Racherla, P. N., Adams, P. J., Pandis, S. N., Impact of climate
636 change on mercury concentrations and deposition in the eastern United States, *Sci. Total*
637 *Environ.*, 487, 299-312, doi: 10.1016/j.scitotenv.2014.03.084, 2014.
- 638 Nair, U. S., Wu, Y., Walters, J., Jansen, J., Edgerton, E. S.: Diurnal and seasonal variation of
639 mercury species at coastal-suburban, urban, and rural sites in the southeastern United States,
640 *Atmos. Environ.*, 47, 499-508, 2012.
- 641 Peterson, C., Gustin, M., and Lyman, S.: Atmospheric mercury concentrations and speciation
642 measures from 2004 to 2007 in Reno, Nevada, USA, *Atmos. Environ.*, 43(30), 4646-4654.
643 doi:10.1016/j.atmosenv.2009.04.053, 2009.
- 644 Rutter, A. P., Schauer, J. J., Shafer, M. M., Creswell, J., Olson, M. R., Clary, A., Robinson, M.,
645 Parman, A. M., and Katzman, T. L.: Climate Sensitivity of Gaseous Elemental Mercury Dry
646 Deposition to Plants: Impacts of Temperature, Light Intensity, and Plant Species, *Environ.*
647 *Sci. Technol.*, 45(2), 569-575, 2011.
- 648 Selin, N. E.: Global change and mercury cycling: Challenges for implementing a global mercury
649 treaty, *Environ. Toxicol. Chem.*, 33, 6, 1202–1210, 2014.
- 650 Seo, Y.-S., et al.: Characteristics of total gaseous mercury (TGM) concentrations in an industrial
651 complex in South Korea: impacts from local sources, *Atmos. Chem. Phys.*, 16, 10215–
652 10228, 2016.
- 653 Sigler, J. M., Mao, H., and Talbot, R.: Gaseous elemental and reactive mercury in southern New
654 Hampshire, *Atmos. Chem. Phys.*, 9, 1929-1942, 2009.
- 655 Sprovieri, F., Pirrone, N., Ebinghaus, R., Kock, H., and Dommergue, A.: A review of worldwide
656 atmospheric mercury measurements, *Atmos. Chem. Phys.*, 10(17), 8245-8265.
657 doi:10.5194/acp-10-8245-2010, 2010.



- 658 Stamenkovic, J., Lyman, S., and Gustin, M. S.: Seasonal and diel variation of atmospheric
659 mercury concentrations in the Reno (Nevada, USA) airshed, *Atmos. Environ.*, 41, 6662–
660 6672, 2007.
- 661 Stein, A. F., Draxler, R. R., Rolph, G. D., Stunder, B. J. B., Cohen, M. D., and Ngan, F.:
662 NOAA's HYSPLIT atmospheric transport and dispersion modeling system, *Bull. Amer.*
663 *Meteor. Soc.*, 96, 2059-2077, <http://dx.doi.org/10.1175/BAMS-D-14-00110.1>, 2015.
- 664 Wang, Y., Huang, J., Hopke, P. K., Holsen, T. M., Rattigan, O. V., Chalupa, D. C., and Utell, M.
665 J.: Effect of the shutdown of a large coal-fired power plant on ambient mercury species,
666 *Chemosphere*, 92, 360–367, 2013.
- 667 Xu, X., Akhtar, U., Clark, K., and Wang, X.: Temporal Variability of Atmospheric Total
668 Gaseous Mercury in Windsor, ON, Canada, *Atmosphere*, 5, 536-556,
669 doi:10.3390/atmos5030536, 2014.
- 670 Ye, Z., Mao, H., Hogrefe, C., Zhang, Y., and Jaegle, L.: Regional photochemical model
671 evaluation of speciated ambient mercury and mercury wet and dry deposition, to be
672 submitted to *J. Adv. Model. Earth Sys.*, 2017.
- 673 Zhang, L., Wang, S., Wang, L. and Hao, J. M.: Atmospheric mercury concentration and
674 chemical speciation at a rural site in Beijing, China: Implications of mercury emission
675 sources., *Atmos. Chem. Phys.*, 13(20), 10505-10516. doi:10.5194/acp-13-10505-2013, 2013.
- 676 Zhang, L., et al.: The estimated six-year mercury dry deposition across North America, *Environ.*
677 *Sci. Technol.*, doi: 10.1021/acs.est.6b04276, 50, 12864-12873, 2016.
- 678 Zhou, Y., Mao, H., Demerjian, K., Hogrefe, C., and Liu, J.: Baseline carbon monoxide and
679 ozone in the northeast US over 2001–2010, *Atmos. Chem. Phys. Discuss.*, 15, 27253–27309,
680 2015.



681 Zhu, J., Wang, T., Talbot, R., Mao, H., Hall, C. B., Yang, X., and Huang, X.: Characteristics of
682 atmospheric total gaseous mercury (TGM) observed in urban Nanjing, China, Atmos. Chem.
683 Phy., 12(24), 12103, doi:10.5194/acp-12-12103-2012, 2012.

684 Zhu, J., and Liang, X.-Z.: Impacts of the Bermuda High on Regional Climate and Ozone over the
685 United States, J. Clim., 26, 1018-1026, 2013.

686



687
688
689
690
691

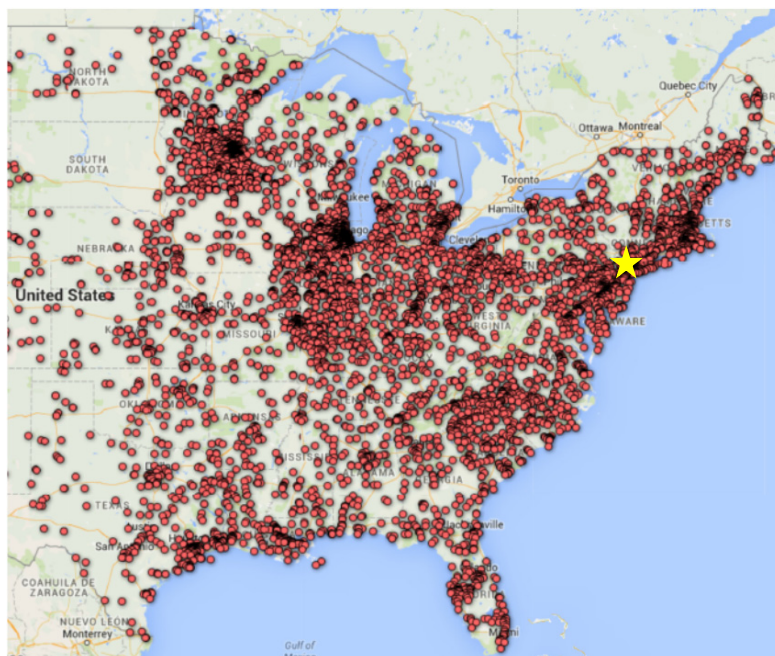


Figure 1. Map of mercury emission sources in the Eastern US.
The yellow asterisk marks the location of the Bronx site.



692
693
694
695
696

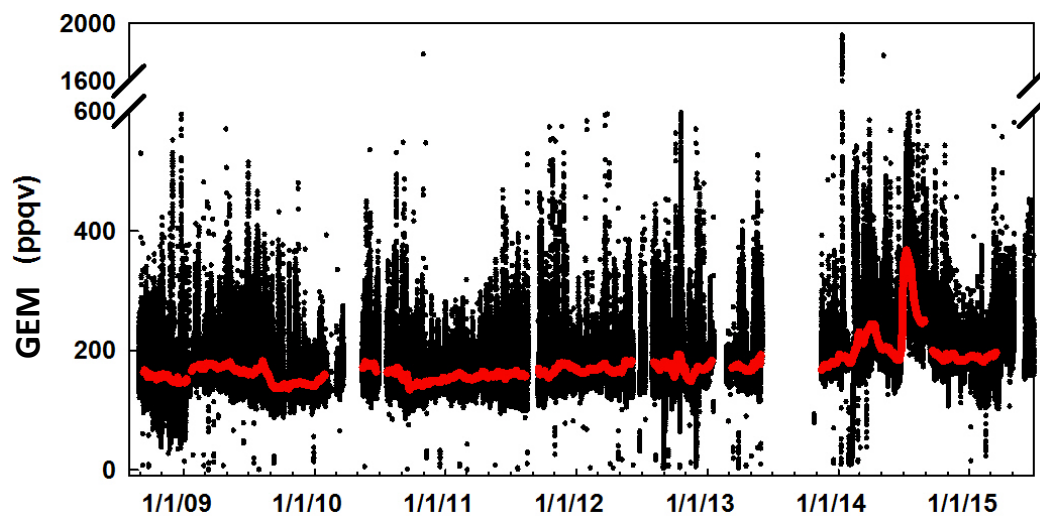


Figure 2. Time series of 5-min average GEM mixing ratios (black dots) with 30-day running average (red line) during the study period.



697 202

698

699

700

701

702

703

704

705

706

707

708

709

710

711

712

713

714

715

716

717

718

719

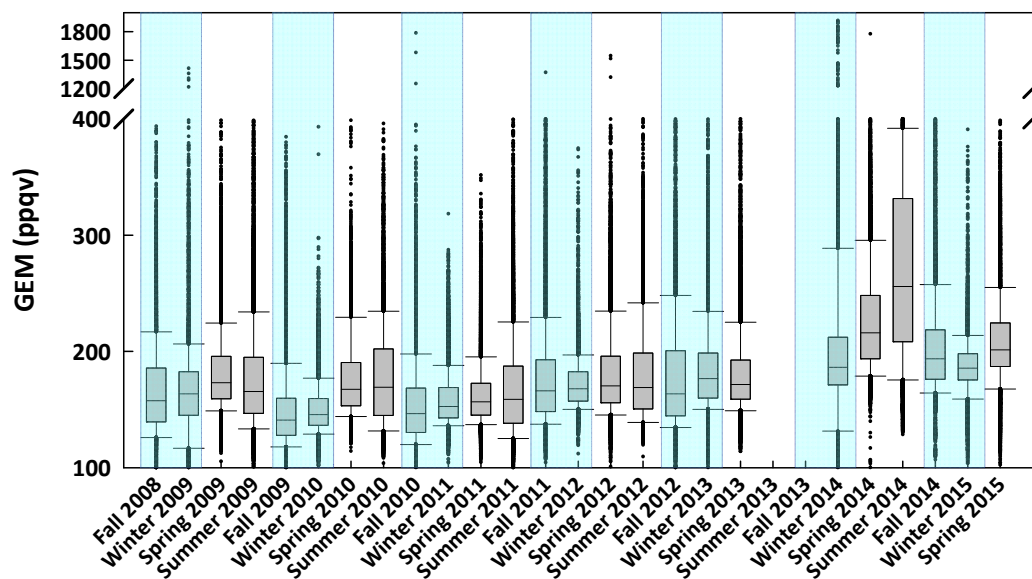
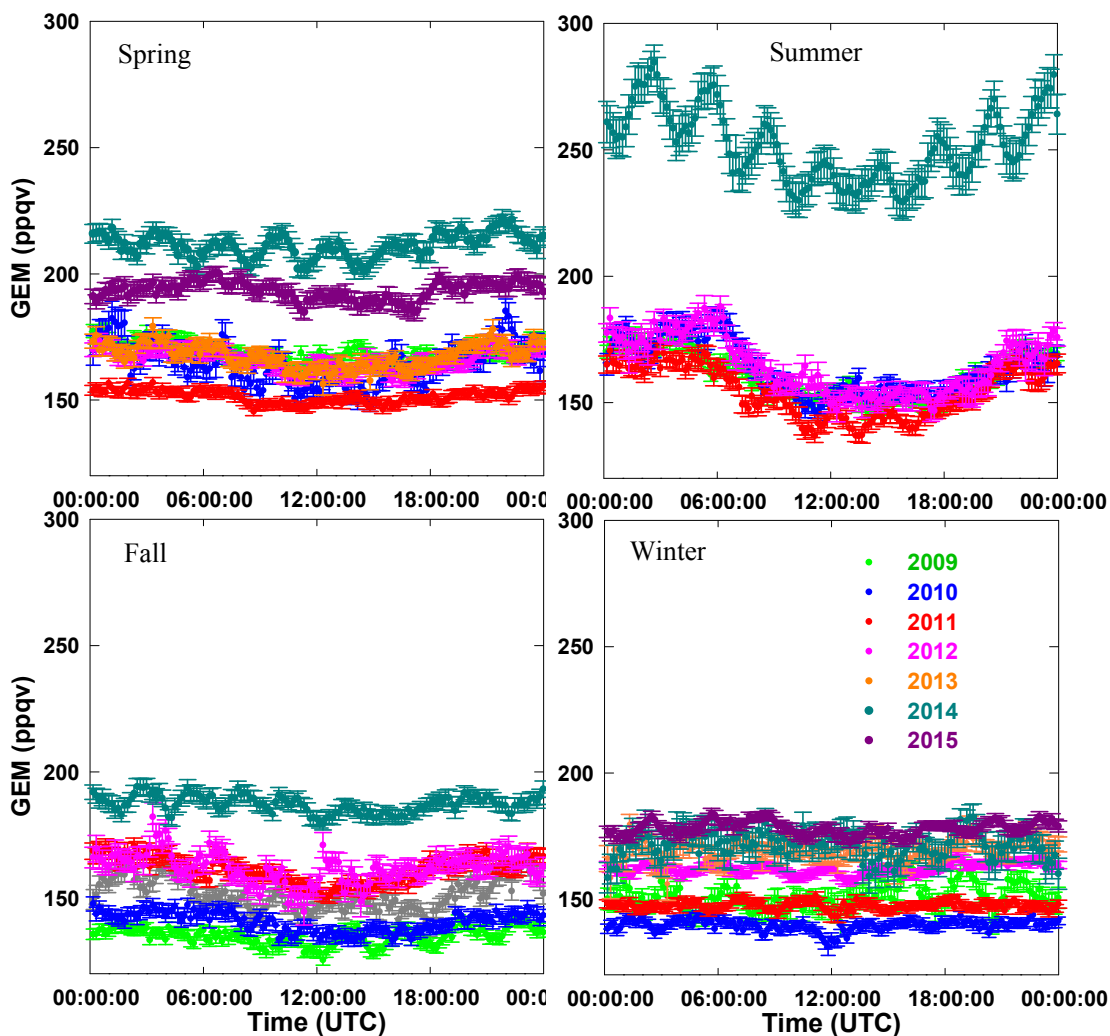


Figure 3. Seasonal 10th, 25th, 50th, 75th, and 90th GEM percentile values. The blue shaded areas are the cool seasons.



720
721
722
723
724
725
726
727
728
729
730
731
732
733
734
735
736
737
738
739
740
741
742
743
744
745
746
747
748



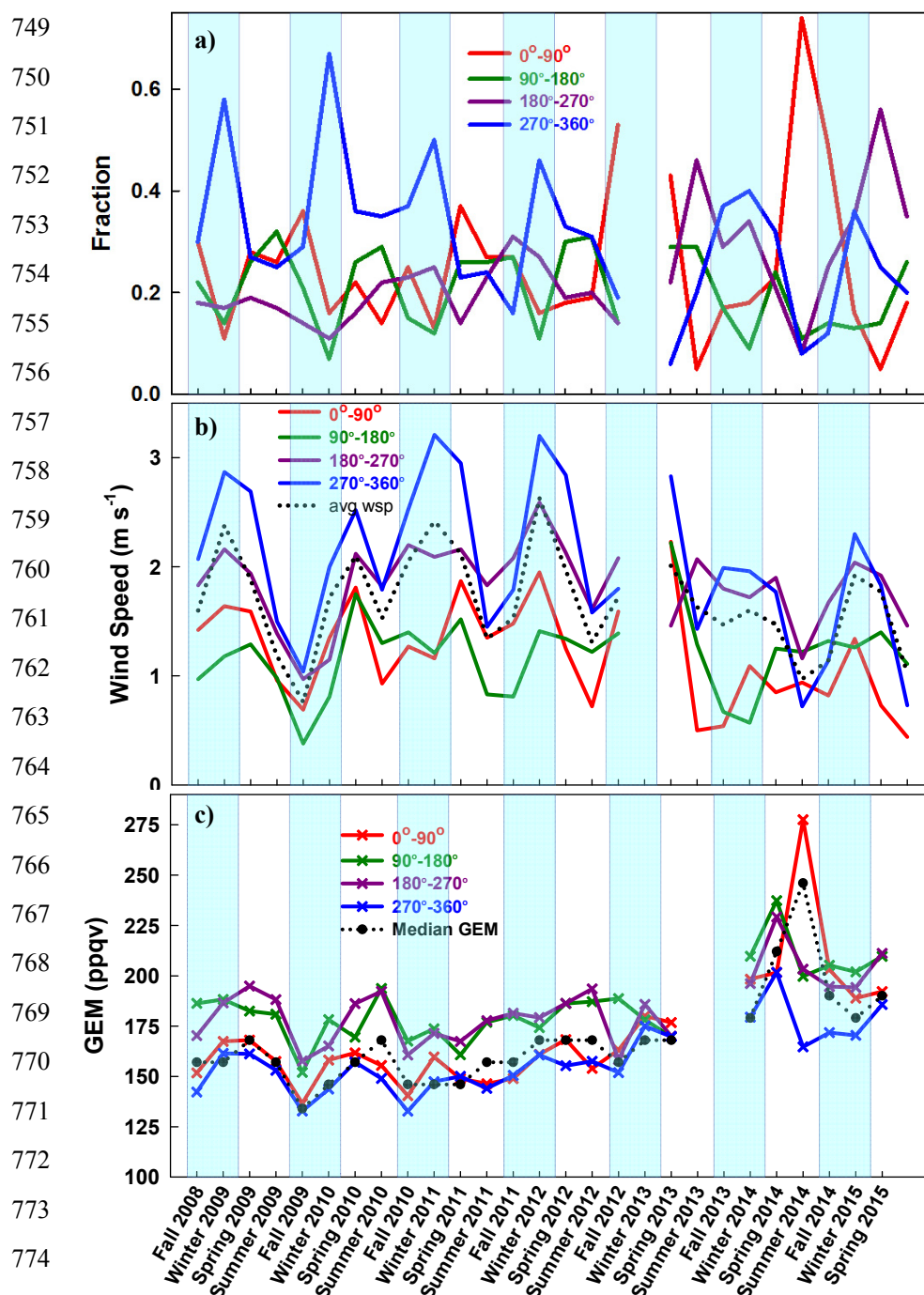


Figure 5. a) Fraction of wind coming from, b) wind speed, and c) TGM averaged in the four wind quadrants in each season. The shaded areas indicate the cool seasons. In b) the black dotted line indicates the wind speed averaged in all directions. In c) the black dotted line and black solid dots represent the overall median values of GEM.



777
 778
 779
 780
 781
 782

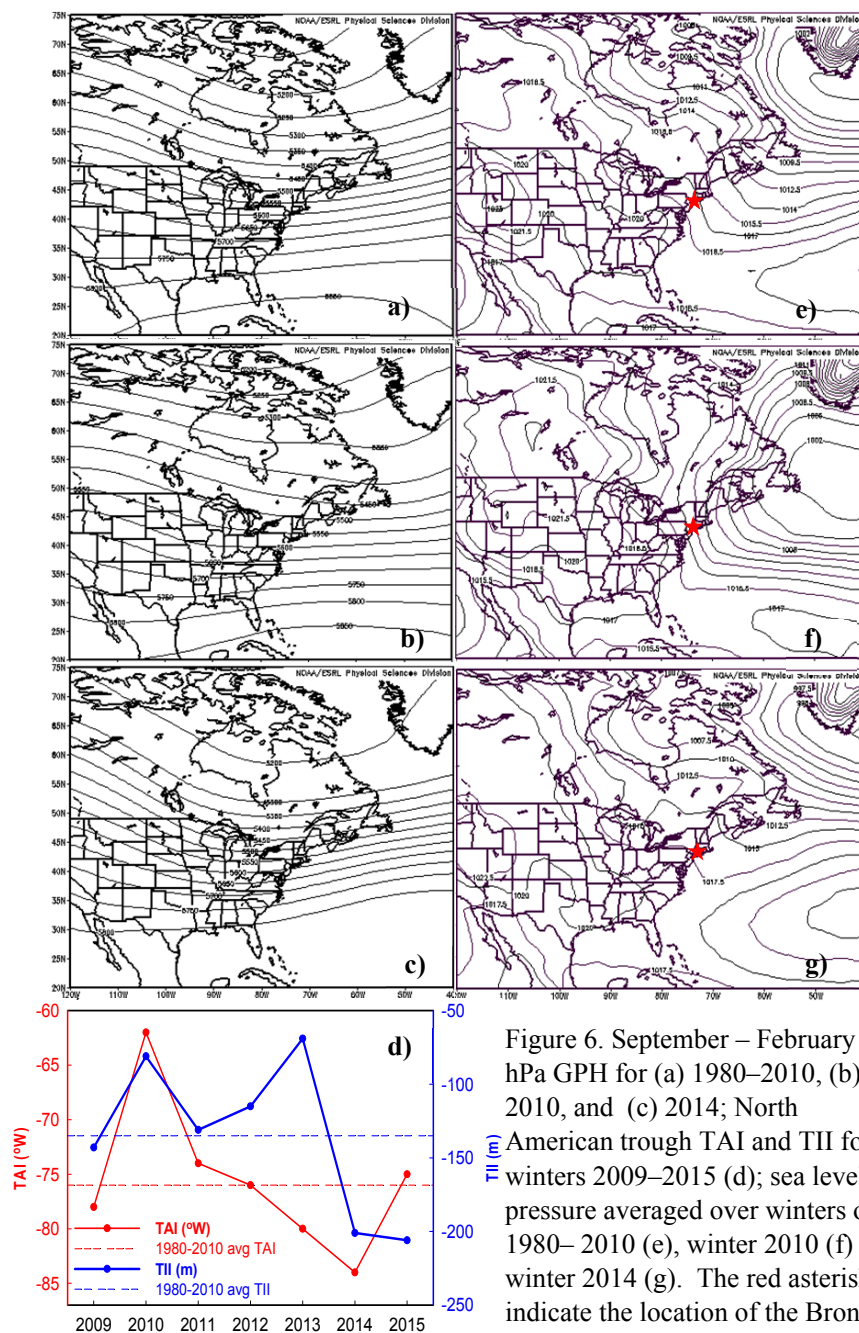


Figure 6. September – February 500 hPa GPH for (a) 1980–2010, (b) 2010, and (c) 2014; North American trough TAI and TII for winters 2009–2015 (d); sea level pressure averaged over winters of 1980–2010 (e), winter 2010 (f) and winter 2014 (g). The red asterisks indicate the location of the Bronx site. (Courtesy: NOAA ESRL PSD Interactive Climate Analysis).



783

784

785

786

787

788

789

790

791

792

793

794

795

796

797

798

799

800

801

802

803

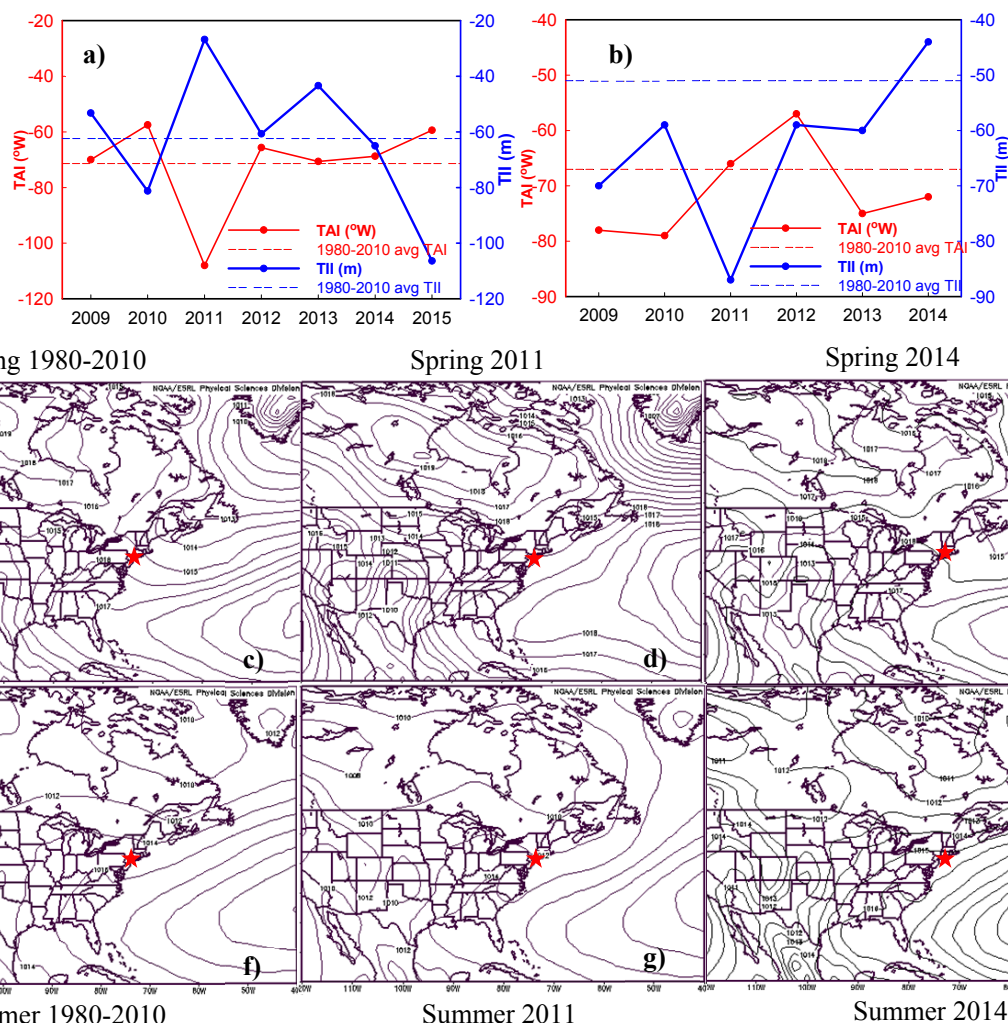


Figure 7. The axis position (TAI) and intensity (TII) of the 500 hPa North American Trough in spring (a) and summer (b). Sea level pressure (SLP) in spring (c) 1980-2010, (d) 2011, and (e) 2014. SLP in summer (f) 1980 – 2010, (g) 2011, and (h) 2014. The red asterisks indicate the Bronx site location. (Courtesy: NOAA ESRL PSD Interactive Climate Analysis)



807
 808
 809
 810
 811
 812
 813
 814
 815
 816
 817
 818
 819
 820
 821
 822
 823
 824
 825
 826
 827
 828
 829
 830

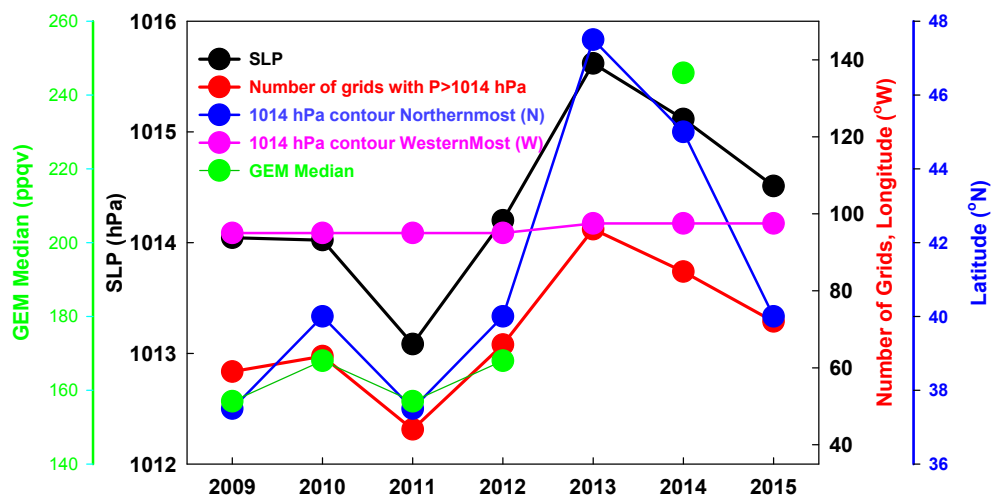


Figure 8. Average sea level pressure (SLP) over the domain of 25°N-50°N, 95°W-70°W (black), number of grids with SLP > 1014 hPa (red), the northernmost latitude (blue) and the westernmost longitude (magenta) the 1014 hPa SLP contour reached, and seasonal median GEM mixing ratios (green) in the summer.



831

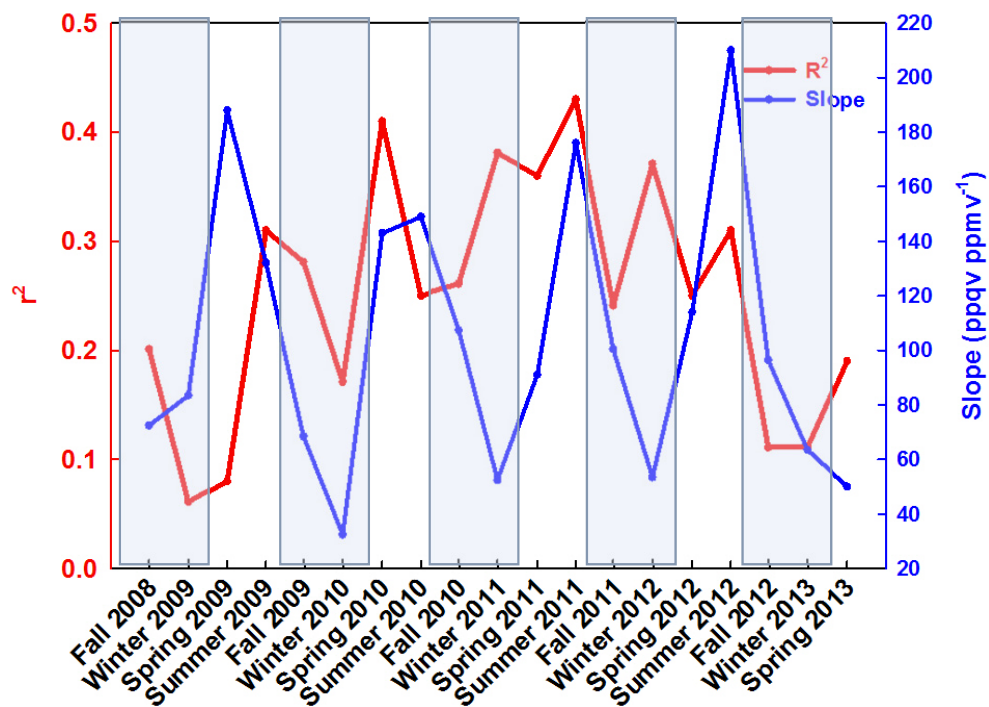


Figure 9. Values of r^2 (red) and slope (blue) of GEM-CO correlation during each season from 2008 to 2013. All r^2 values were statistically significant with p approaching 0.



832

833

834

835

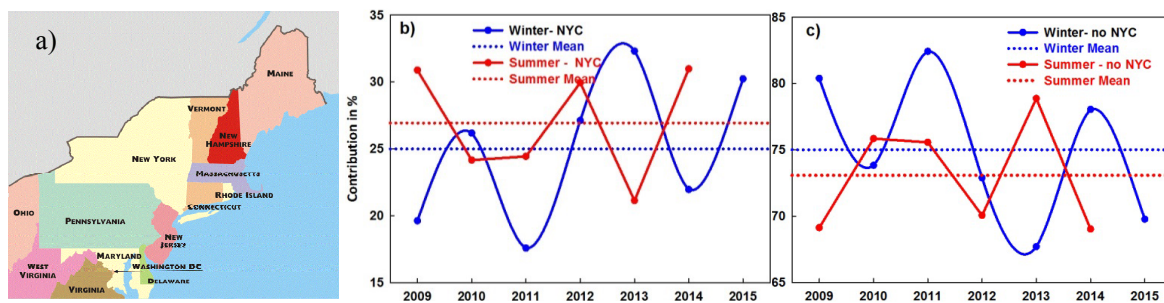


Figure 10. a) Counties and states that contributed to Hg in NYC; b) Contributions (in %) of NYC sources to NYC Hg concentrations; c) Contributions (in %) of sources outside of NYC to NYC Hg concentrations in winter (blue) and summer (red).



836 Table 1. Seasonal statistic metrics of GEM mixing ratios from the Bronx site.

		10th	25th	Median	75th	90th	Range	Sample #
2008	Fall	123	134	157	179	213	22-963	14900
2009	Winter	112	134	157	179	202	11-7302	9861
	Spring	146	157	168	190	224	11-15310	15129
	Summer	123	146	157	190	224	11-515	15577
	Fall	112	123	134	157	179	11-470	13291
2010	Winter	123	134	146	157	168	11-392	10414
	Spring	134	146	157	190	224	56-448	4383
	Summer	123	134	168	201	224	78-526	9303
	Fall	112	123	146	168	190	11-1781	12245
2011	Winter	134	134	146	168	179	11-314	15364
	Spring	134	134	146	168	190	34-784	15653
	Summer	123	134	157	179	224	22-526	12548
	Fall	134	146	157	190	224	22-3886	12949
2012	Winter	146	157	168	190	224	11-1064	15264
	Spring	134	146	168	190	224	11-1546	13888
	Summer	134	146	168	190	235	11-2766	8406
	Fall	134	142	157	190	246	11-896	13210
2013	Winter	146	157	168	190	224	11-1064	7905
	Spring	146	157	168	190	224	11-526	12124
	Summer	-	-	-	-	-	-	-
	Fall	-	-	-	-	-	-	-
2014	Winter	134	168	179	202	280	11-1915	14709
	Spring	168	190	212	246	291	34-1770	15317
	Summer	168	202	246	325	392	123-1064	13161
	Fall	157	168	190	213	246	101-538	12847
2015	Winter	157	168	179	190	213	11-381	15250
	Spring	157	179	190	224	246	101-795	11124

837



838 Table 2. Pearson correlation coefficients (r) between GEM and SO₂ and between GEM and NO₂
 839 with p values in parenthesis, for seasons during fall 2008 - spring 2015.

	All data		SO ₂ & NO ₂ > 95 th percentile	
	SO ₂	NO ₂	SO ₂	NO ₂
Fall 2008	-0.04 (=0.0675)	0.28 (<0.0001)	0.08 (=0.471)	-0.03 (=0.810)
Winter 2009	0.14 (<0.0001)	0.29 (<0.0001)	-0.21 (=0.0877)	-0.05 (=0.687)
Spring 2009	0.08 (=0.0006)	0.22 (<0.0001)	-0.02 (=0.832)	0.09 (=0.41)
Summer 2009	0.15 (<0.0001)	0.43 (<0.0001)	0.50 (<0.0001)	0.25 (=0.0152)
Fall 2009	0.22 (<0.0001)	0.50 (<0.0001)	-0.29 (=0.0067)	-0.03 (=0.776)
Winter 2010	0.36 (<0.0001)	0.49 (<0.0001)	0.06 (=0.592)	0.07 (=0.569)
Spring 2010	0.03 (=0.549)	0.34 (<0.0001)	-0.13 (=0.507)	0.13 (=0.505)
Summer 2010	0.10 (<0.0001)	0.45 (<0.0001)	-0.07 (=0.605)	0.22 (=0.105)
Fall 2010	0.09 (=0.0005)	0.35 (<0.0001)	-0.01 (=0.929)	-0.06 (=0.567)
Winter 2011	0.44 (<0.0001)	0.64 (<0.0001)	-0.23 (=0.0267)	-0.04 (=0.670)
Spring 2011	0.01 (=0.706)	0.36 (<0.0001)	0.01 (=0.901)	0.24 (=0.0156)
Summer 2011	0.15 (<0.0001)	0.48 (<0.0001)	-0.12 (=0.285)	0.11 (=0.296)
Fall 2011	0.20 (<0.0001)	0.48 (<0.0001)	0.19 (=0.0839)	0.20 (=0.0685)
Winter 2012	0.18 (<0.0001)	0.51 (<0.0001)	0.11 (=0.285)	0.11 (=0.278)
Spring 2012	0.10 (<0.0001)	0.40 (<0.0001)	-0.12 (=0.268)	-0.16 (=0.125)
Summer 2012	0.13 (<0.0001)	0.24 (<0.0001)	-0.10 (=0.475)	0.02 (=0.903)
Fall 2012	-0.18 (<0.0001)	0.08 (=0.0005)	-0.34 (=0.0011)	-0.37 (=0.0004)
Winter 2013	0.09 (=0.0021)	0.37 (<0.0001)	-0.22 (=0.102)	-0.29 (=0.0282)
Spring 2013	-0.02 (=0.478)	0.43 (<0.0001)	0.03 (=0.786)	0.38 (=0.0004)
Summer 2013	N/A	N/A	N/A	N/A
Fall 2013	N/A	N/A	N/A	N/A
Winter 2014	-0.15 (<0.0001)	0.01 (=0.638)	-0.25 (=0.0154)	0.05 (=0.638)
Spring 2014	0.05 (=0.0167)	0.35 (<0.0001)	0.05 (=0.608)	0.05 (=0.654)
Summer 2014	0.12 (<0.0001)	0.26 (<0.0001)	-0.15 (=0.167)	0.08 (=0.449)
Fall 2014	-0.12 (=0.0001)	0.33 (<0.0001)	0.05 (=0.612)	0.05 (=0.608)
Winter 2015	0.26 (<0.0001)	0.57 (<0.0001)	0.02 (=0.835)	0.03 (=0.816)
Spring 2015	0.12 (<0.0001)	0.48 (<0.0001)	0.05 (=0.656)	0.07 (=0.557)

840

841

842

843

844

845

846